The British Journal of Radiology, 84 (2011), S145–S158

Imaging hypoxia in gliomas

I MENDICHOVSZKY, MD, PhD and A JACKSON, PhD, FRCR

Wolfson Molecular Imaging Centre, University of Manchester, Manchester, UK

ABSTRACT. Hypoxia plays a central role in tumour development, angiogenesis, growth and resistance to treatment. Owing to constant developments in medical imaging technology, significant advances have been made towards *in vitro* and *in vivo* imaging of hypoxia in a variety of tumours, including gliomas of the central nervous system. The aim of this article is to review the literature on imaging approaches currently available for measuring hypoxia in human gliomas and provide an insight into recent advances and future directions in this field. After a brief overview of hypoxia and its importance in gliomas, several methods of measuring hypoxia will be presented. These range from invasive monitoring by Eppendorf polarographic O_2 microelectrodes, positron electron tomography (PET) tracers based on 2-nitroimidazole compounds [^{18}F-labelled fluoromisonidazole (^{18}F-MISO) or 1-(2-[(^{18})F]fluoro-1-[hydroxymethyl]ethoxy)methyl-2-nitroimidazole (FRP-170)], ^{64}Cu-ATSM Cu-diacetyl-bis(N4-methylthiosemicarbazone) (Cu-ATSM) or ^{99m}Tc- and ^{68}Ga-labelled metronidazole (MN) agents to advanced MRI methods, such as blood oxygenation level dependent (BOLD) MRI, oxygen-enhanced MRI, diffusion-weighted MRI (DWI-MRI), dynamic contrast-enhanced MRI (DCE-MRI) and ^{1}H-magnetic resonance spectroscopy.

DOI: 10.1259/bjr/82292521

Mounting evidence over the last decade indicates that hypoxia plays a vital role in tumour development, angiogenesis, growth and resistance to treatment. Alterations in the malignant potential of tumours induced by hypoxia and changes in the tumour's gene expression lead to more aggressive survival patterns and result in resistance to radiation, photodynamic therapy and cytotoxic chemotherapy [1]. Hypoxia imaging may help select the patients who would be most likely to benefit from novel hypoxia-directed therapies and increase our understanding of the role tissue hypoxia plays in tumour biology.

Overview of hypoxia and its importance

In solid tumours, the vascular system fails to supply the rapidly growing tumoural mass with adequate amounts of oxygen, resulting in low oxygen tensions, nutrient deprivation and hypoxia. The major factors in the development of tumour cell hypoxia are structural and functional abnormalities in the tumoural microvasculature [2], increased diffusion distances between blood vessels, growing competition for oxygen between different regions of the expanding tumour cell mass and the reduced oxygen carrying capacity of blood due to disease- or treatment-related anaemia.

Three distinct types of tumour hypoxia can be identified [3]. (1) Acute (perfusion-related) hypoxia results from inadequate blood supply to and within tumours, a consequence of recognised structural and functional abnormalities of the tumour neovasculature. Acute hypoxia is often transient, caused by temporary occlusions and temporary rises in interstitial pressure and can affect vessels both in the vicinity and far from the vessel wall. (2) Chronic (diffusion-related) hypoxia is caused by the increase in diffusion distances of oxygen relative to the supplying blood vessel due to tumour expansion and affects cells at distances greater than 70–100 μm from the nearest capillary. This type of hypoxia also depends on where tumour cells lie in relation to the arterial or venous end of a capillary. (3) Anaemic hypoxia relates to reduced O_2-carrying capacity of the blood and may be tumour associated or treatment related.

Hypoxia measurements have been shown to correlate with the probability of metastatic spread [4], tumour recurrence [5], resistance to chemotherapy and radiation [6–9], invasion [10, 11] and decreased patient survival [12, 13]. A few studies suggested hypoxia-induced phenotypic changes, such as genomic instability, loss of apoptotic potential, alterations of gene expression, oncogene activation and induction of angiogenesis, are necessary conditions to malignant progression [14–20].

The critical level below which intratumoural partial oxygen pressure (pO_2) changes result in impaired cellular metabolism across tumoural cell types is still hotly debated. Establishing a pO_2 threshold is difficult because experimental findings in cell cultures may not be directly applied to *in vivo* environments and some of the variation in the published literature can be related to the tumour cell type and the demands of host tissues. The approximate values of critical pO_2 below which cellular functions progressively cease or anticancer treatments become less effective have been established as follows [21]:

- effectiveness of immunotherapy becomes impaired (30–35 mmHg);

Address correspondence to: Dr Alan Jackson, Wolfson Molecular Imaging Centre, 27 Palatine Road, Withington, Manchester M20 3LJ, UK. E-mail: Alan.Jackson@Manchester.ac.uk

- photodynamic therapy (15–35 mmHg);
- cell death on exposure to radiation (25–30 mmHg);
- binding of hypoxia immunohistochemical markers (10–20 mmHg);
- proteome changes (1–15 mmHg);
- genome changes (0.2–1 mmHg).

A large amount of clinical evidence suggests the hypoxia-mediated aggressive behaviour of cancer cells and their resistance to therapy is mediated by the hypoxia inducible factor-1 α (HIF-1α) through numerous molecular pathways required for the adaptation of tumour cells to hypoxia [22]. The emergence of new and more aggressive cell clones capable of overcoming nutrient deprivation and their hostile environments is facilitated by hypoxia-induced adaptations in the proteome and genome of neoplastic cells. Hypoxia initiates the selection of more aggressive cell types that, in turn, results in exacerbation of regional hypoxia, with development of further resistance to chemotherapy and radiotherapy. HIF-1α overexpression is described in a host of human cancers: prostate [23], squamous cell carcinoma [24], lung [25], breast [26, 27], bladder [28] and pancreas [29]. Several studies have also demonstrated that increased HIF-1α activity is a predictor of a more aggressive tumour grade, tumour invasion, resistance to radiation therapy, metastatic potential, and is associated with a poorer prognosis [26, 30–36]. Cell lines genetically altered to knock down HIF-1α show decreased cell growth both *in vivo* and *in vitro* [37–40].

Glioma cell lines *in vitro* overexpress HIF-1α in both normoxic and hypoxic conditions, so that most malignant glioma cell lines have increased vascular endothelial growth factor (VEGF) and HIF-1α expression at baseline [41–45]. Several other HIF-1α downstream-regulated proteins and their association with cancer is less known, although CA-IX and Glut-1 expression has been reported to correlate with poor response to adjuvant treatments [46–48]. Overexpression of CA-IX and Glut-1 has been established in higher-grade brain tumours [41, 49–57] and malignant glioma cell lines [56, 58], whereas CA-IX expression in malignant gliomas has been shown to predict radiological response and survival of patients treated with bevacizumab and irinotecan [59]. High-grade gliomas were also more likely to be immunohistochemically positive for HIF-1α, VEGF, Glut-1 and CA-IX than are low-grade tumours [41, 49].

Several studies have described genetic instability and amplification, disruption of apoptotic pathways, abnormal oncogene expression and abnormal angiogenesis in high-grade gliomas [15, 60–67]. There are several reasons to believe that hypoxia plays a role in high-grade glioma [glioblastoma multiforme (GBM)] development, angiogenesis and growth, the most obvious being the presence of intratumoural necrosis. Animal glioma model studies have shown that while small tumours (<1 mm in diameter) are intensely hypoxic and poorly perfused, large tumours (1–4 mm in diameter) are rich in vasculature and not significantly hypoxic, indicating that tumour necrosis is not simply due to inadequate vascular supply [17, 68]. In spite of being highly vascular, the microcirculation in GBMs is inefficient and may contribute to relative hypoxia and necrosis within a given tumour [69–73]. Measurements of intratumoural hypoxia using direct and indirect methods and attempts at correlating this with tumour blood flow and necrosis have not provided an answer to this controversy [74–77]. Several studies have also found that tumour cells found in the areas surrounding the necrotic centres are implicated in hypoxia-regulated migration away from necrotic areas [78–80], suggesting tumour hypoxia results in increased GBM cell migration and possibly invasion [81–83].

Chemotherapy is clinically useful in the treatment of patients with GBM [84, 85], and GBM chemoresistance is thought to be hypoxia related [86, 87]. Inhibiting hypoxia-regulated survival mechanisms, by stopping the expression of HIF-1α, renders these malignant cells more sensitive to doxorubicin and etoposide [86]. Experiments on malignant glioma cell lines found these cells secrete proteins that suppress hypoxia-induced endothelial cell apoptosis and promote the angiogenic process [88].

Radiation therapy is also extensively used in the treatment of human GBMs [89, 90]. Hypoxia-induced radioresistance is multifactorial with the presence of oxygen mediating DNA damage through the formation of oxygen free radicals, occurring after the interaction of ionising radiation with intracellular water [91]. Accumulating evidence shows hypoxia-mediated proteomic and genomic changes are likely to contribute towards tumoural radioresistance by increasing the levels of heat shock proteins (HSPs). HSPs are induced in response to environmental stresses like heat, cold and oxygen deprivation [17] or by increasing the number of tumour cells that can resist apoptosis by mutating a protein brake called p53. A large proportion (50–55%) of human cancers involve disruptions in the function of p53, and these could be, at least partially, hypoxia related. There is also strong evidence hypoxia makes GBM tumoural cells radioresistant and the intensity of hypoxia in GBM before radiotherapy is associated with decreased time to tumour progression or overall patient survival [92–94].

Tissue oxygenation status can be assessed *in vivo*, using both invasive and non-invasive methods, or *in vitro* using material from a biopsy. Non-imaging methods of assessing the presence of hypoxia in tissues include histological appearance, immunohistochemical staining for intrinsic markers of hypoxia (*e.g.* CA-IX and HIF-1α) and for the binding of externally administered nitroimidazoles [91, 95–97]. Hypoxic cancer cells, both human and animal, can be labelled using nitroimidazole derivatives, such as EF5 and pimonidazole [98–100]. In a low O_2 concentration environment, nitroimidazole molecules are bioreduced by nitroreductases, bind to cellular macromolecules and are trapped intracellularly [101, 102]. EF5- and pimonidazole-specific antibodies can be used to measure these molecules using various immunohistochemical methods [99, 100, 103, 104]. Other methods of measuring intratumoural hypoxia are the use of polarographic O_2 microelectrodes and advanced PET and MRI. Measurement of tumour hypoxia is even more challenging in a clinical setting and there is no easy way to predict its presence or readily measure it. Imaging is one possible way of non-invasively selecting cancer patients who would benefit from treatments that take advantage of the presence of hypoxia. Since tumour hypoxia plays a key role in radioresistance, it has been suggested hypoxia

mapping could be combined with radiotherapy techniques to improve target delineation and dose delivery. Imaging could also be used to document the extent to which re-oxygenation of tumours occurs during radiotherapy and the heterogeneity between and within tumours.

An ideal imaging test should:

(1) distinguish normoxia, hypoxia, anoxia or necrosis;
(2) distinguish between perfusion-related (acute) and diffusion-related (chronic) hypoxia;
(3) reflect cellular, in preference to vascular/extracellular, pO_2;
(4) be applicable to any tumour site with complete locoregional evaluation;
(5) be simple to perform, non-toxic and allow repeated measurements; and
(6) be sensitive at pO_2 levels relevant to tumour therapy [105].

The challenge for hypoxia imaging is to measure low levels of tissue pO_2 on a small spatial scale (70–100 μm), a much smaller dimension than can be achieved with current human imaging techniques.

Several methods have been proposed and evaluated for clinical imaging of hypoxia and only a few techniques have potential for *in vivo* assessment in humans, particularly for repeated, sequential measurements. These methods use either PET tracers [^{18}F-fluoromisonidazole (^{18}F-MISO) and $^{60/64}$Cu-ATSM PET being the most common ones used] or MRI techniques sensitive to variations in local oxygen changes [such as blood oxygenation level dependent MRI (BOLD-MRI) or dynamic contrast-enhanced MRI (DCE-MRI)].

Eppendorf O_2 microelectrodes

Measuring intratumoural hypoxia is a difficult task and the only method for direct and invasive measurements is to use Eppendorf polarographic O_2 microelectrodes (POEs) for spatial mapping of tumour hypoxia in experimental models. This technique has been used in various tumour types to demonstrate tumour hypoxia, but its use was limited in human brain tumour studies [76, 104, 106–110].

The studies that have shown positive relationships between Eppendorf oxygen probe measurements and treatment outcomes have used different endpoints when making measurements. Estimating the median pO_2 or a range of pO_2 values across a tumour requires many measurements, whereas stratifying patients into diagnostic categories based on median pO_2 requires fewer. One study reported that 20 independent measurements are necessary to classify tumours as oxic or hypoxic and to reduce the proportion of false classifications [111].

The use of hypoxic biomarkers in routine clinical practice has been slow due to the invasive nature of the electrodes and by the inability to specifically target hypoxic tumour regions of variable size and location during the course of treatment [112]. Concurrent HIF-1α expression and pimonidazole staining of U87 glioma cell lines has been demonstrated *in vitro* but not in tumour xenograft experiments [104, 113]. HIF-1α, CA-IX and Glut-1 expression are inversely distributed relative to vascular perfusion and correlate with POE and pimonidazole staining in many tumour types. However, this relationship has not been proven in GBM [47, 114–117].

The difficulty in using biomarkers as a clinical tool is the inability to determine which hypoxia-regulated protein or method provides the best ''hypoxia marker'' [114, 118]. There are also questions surrounding which of these molecules and methods can measure ''real-time'' or ''acute'' hypoxia as opposed to cumulative cellular hypoxia [104]. The lack of direct correlation between POE measurements, biochemical data and imaging studies (discussed in the next section) has contributed to the confusion of the role of hypoxia in GBM.

In spite of their limitations, Eppendorf probe measurements are commonly considered a gold standard for hypoxia, but in reality, it is difficult to determine which technique is the best. One technique might be preferable in mapping absolute oxygen values in tumours, whereas another could be better for clinical trials testing hypoxia-dependent drug effects. Furthermore, all techniques available to measure hypoxia differ in sensitivity, accuracy and ability to measure oxygen availability. While pO_2 histography and electron paramagnetic resonance (EPR) measure oxygen availability directly, others provide information indirectly through reduced drug levels, haemoglobin saturation or perfusion. Direct measurements rely on measuring collision rates, which depend on oxygen concentration and diffusion, as well as on the type of probe used. Indirect measurements, although valuable, require a set of assumptions to relate the measurement to pO_2 or oxygen concentration. The Eppendorf electrode is primarily an extracellular measurement and does not distinguish between acute and chronic hypoxia or between hypoxic and necrotic tissue.

Positron emission tomography

Ideally, nuclear medicine techniques should allow the evaluation of both chronic and transient hypoxia and reflect cellular pO_2 without contamination by vascular signals. They should be simple, use non-toxic radiopharmaceuticals and be repeatable. They should also provide complete locoregional evaluation with a spatial resolution adequate for assessing the heterogeneity of local pO_2. For the patient's convenience, nuclear medicine techniques should permit imaging on the same day the radiopharmaceutical is administered and short half-life isotopes should be used to minimise radiation exposure.

Human PET imaging of 2-nitroimidazole compounds, such as ^{18}F-MISO, has been used to identify hypoxic tumours (including gliomas) [106, 119–124]. ^{18}F-MISO is probably the most widely used PET imaging agent for hypoxia. ^{18}F-MISO can be generated by using a commercially available precursor molecule and is adaptable to existing PET technology for automated radiosynthesis. Clinically, PET ^{18}F-MISO is a well-tolerated procedure by patients and takes around 20–30 min, starting from 75 to 150 min after injection and making it similar to the bone scan with which most cancer patients are familiar. Radiation dose is low, typically 250 MBq, and no arterial sampling or metabolite analysis is required. The initial

^{18}F-MISO uptake, within 5 min after injection, correlates tightly with blood flow [125]. After an hour, the F-MISO–plasma ratio is unity for most normoxic tissues, consistent with the partition coefficient of ^{18}F-MISO. Similar ratios are observed in experiments in mice, rats, guinea pigs, dogs and humans. A tumour-blood ratio of 1.2 has been demonstrated as a reasonable cut-off between normoxia and hypoxia. Hypoxia can be detected in the presence of normal or reduced blood flow, and the absence of hypoxia can be detected with flow that is only one-third normal. ^{18}F-MISO images can be acquired 1 h after tracer injection, but best contrast will be achieved 90–150 min post injection.

Quantitatively, the degree of hypoxia can be defined by hypoxic fraction or volume, or can be expressed by its severity, defined as the region with the lowest oxygen concentration and its relative level. Calculating the hypoxic tumour fraction (percentage of pixels with values greater than the tumour–blood cut-off of 1.2) requires accurate delimitation of the tumoural volume. PET ^{18}F-MISO imaging studies cannot provide values of regional oxygen concentration, but the maximum tumour–blood ratio is a convenient surrogate for the worst level of hypoxia in the image. It remains to be established whether a larger hypoxic volume, a more severe hypoxic area or heterogeneity of the hypoxic region is the strongest predictor of response to cancer treatment [91].

PET imaging with ^{18}F-MISO has several advantages. Early ^{18}F-MISO distribution reflects blood flow, while later distribution is purely a measure of tissue–plasma partitioning. ^{18}F-MISO diffuses freely across the blood–brain barrier, is reduced at any hypoxic site where it is not excreted or highly metabolised and its metabolites have a rapid plasma clearance, so normalisation for delivery is not required. ^{18}F-MISO has no protein binding and imaging is possible within 90–120 min of ^{18}F-MISO administration. Further advantages are that ^{18}F-MISO has been validated in several animal models and human disease conditions, and its signal is independent of other factors associated with hypoxia, such as regional glucose concentration, glutathione levels, other transporters and pH [91].

Limitations of ^{18}F-MISO PET include the low signal-to-noise ratio (SNR) of raw ^{18}F-MISO PET images, large range of fractional hypoxic volume values across tumour types (making standard correlation of hypoxic volume with that of the tumour difficult) and serial measurements can only be performed more than a day apart, limiting the ability of ^{18}F-MISO PET to monitor temporal heterogeneity of tumour function. The low SNR can be improved by taking a venous blood sample during the mid-course of the imaging procedure and used to calculate a tumour–blood (T/B) ratio image and then electronically subtracting the normoxic uptake (T/B$<$1) to increase image contrast.

A recent study in GBM patients imaged pre-operatively using ^{18}F-MISO showed positive correlations between relative hypoxia (defined as the ratio of the hypoxic volume to the MRI T_2 defined tumour volume) and the net rate of cell proliferation, as well as between the biological aggressiveness ratio (defined as the ratio between the net rate of cell proliferation and the net rate of invasion) and relative hypoxia, scaled to the blood activity of the tracer [126]. ^{18}F-MISO and ^{15}O-H_2O PET have also been used in brain tumours to measure tumour hypoxia and perfusion [119]. Increased ^{18}F-MISO brain tumour retention on a delayed scanning time was found predominantly in GBM (7 out of 7) and this was associated with an increased ^{18}F-MISO tumour distribution volume, which was also used as a quantitative criterion for hypoxia. ^{18}F-MISO accumulated in both hypo- and hyperperfused tumour regions, suggesting hypoxia in glioblastoma may develop irrespective of the magnitude of perfusion (Figure 1).

^{18}F-MISO PET was also evaluated in advanced head and neck cancer during hypoxia-targeting therapy. All sites of corresponding fluorodeoxyglucose (FDG) and ^{18}F-MISO abnormality at baseline showed marked qualitative reduction of uptake within 4 weeks of commencing therapy, consistent with effective hypoxia-targeted therapy. The high prevalence of hypoxia demonstrated on ^{18}F-MISO PET imaging was consistent with the advanced disease stage of these patients and predicted adverse prognosis.[127] Another study [128] showed ^{18}F-MISO uptake was present in all high-grade gliomas but not in low-grade gliomas (LGGs). In the same study, a significant relationship was found between FDG or ^{18}F-MISO uptake and expression of vascular endothelial growth factor (VEGF)-R1 and Ki-67 expression. The authors concluded that ^{18}F-MISO PET provides a non-invasive assessment of hypoxia in glioma and is prognostic for treatment outcomes in the majority of patients. There was a correlation between ^{18}F-MISO uptake and tumour grade, and all high-grade lesions showed uptake that was frequently heterogeneous. There was only partial overlap between regions of ^{18}F-MISO uptake and FDG uptake (Figure 2).

Although promising, the above-mentioned studies need to be extended to larger patient trials with serial imaging and follow-up to establish the full clinical potential of ^{18}F-MISO PET in gliomas. Possible applications could include pre-surgical planning to identify the regional distribution of hypoxia and accurate targeting of higher doses of radiotherapy to hypoxic areas of the tumour.

^{18}F-MISO autoradiography correlates with pimonidazole (cellular hypoxia marker) studied by immunohistochemistry in human xenograft tumours [129]. In GBMs imaged by ^{18}F-MISO PET prior to radiotherapy, the volume and intensity of hypoxia showed a strong association with poorer time to tumour progression and overall survival. New treatment strategies to target hypoxia more aggressively in GBM could benefit from ^{18}F-MISO PET imaging, which could also be applied to assess treatment outcomes [94]. Because ^{18}F-MISO is not commonly available at all institutions and has a relatively slow clearance from normoxic tissues, there has been an intense search for newer radiotracers for hypoxia imaging.

Cu-ATSM Cu-diacetyl-bis (N4-methylthiosemicarbazone)

^{64}Cu-ATSM Cu-diacetyl-bis(N4-methylthiosemicarbazone) (Cu-ATSM) is a promising new PET agent for delineating the extent of hypoxia within tumours. Cu-ATSM is retained in hypoxic cells at a higher level than ^{18}F-MISO [130]. Cu-ATSM enters and exits normoxic cells metabolically unchanged, but in hypoxic cells

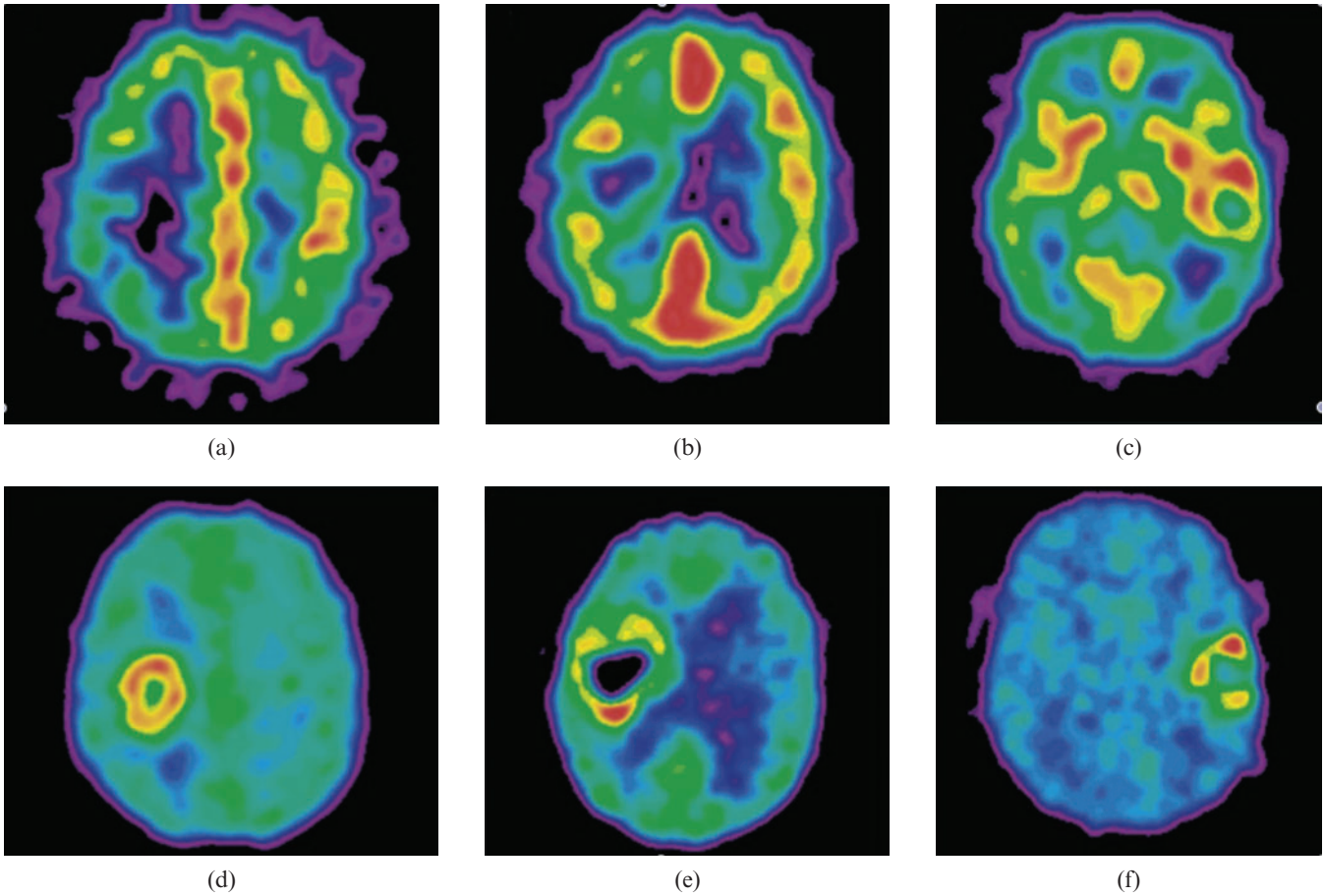

Figure 1. (a–c) ^{15}O-H_2O positron emission tomography (PET) perfusion images in three patients with glioblastoma multiforme. (d–f) Corresponding late ^{18}F-labelled fluoro-misonidazole (^{18}F-MISO) PET images show tumour hypoxia in low perfusion, in intermediate perfusion with an inverse pattern compared with hypoxia and in high perfusion. PET images are normalised to their own maximum. Reproduced with permission from [119].

undergoes alteration and is retained. It is not retained in necrotic tissues. The mechanism of retention of Cu-ATSM in hypoxic tissues is attributed to the low oxygen tensions and the subsequent altered redox environment of hypoxic tumours [increased nicotinamide adenine dinucleotide dehydrogenase (NADH) levels]. Cu-ATSM images hypoxia both in acute ischaemic syndromes where flow is limited and in instances when ischaemia is induced without severe restrictions in flow. With the short-lived copper-PET radionuclides, imaging can be repeated at 120 min intervals, enabling investigators to perform reperfusion studies [91].

Cu-ATSM was validated as a hypoxia PET marker by comparing autoradiographic distributions of Cu-ATSM with a well-established hypoxia marker drug, EF5, in animal R3230 mammary adenocarcinomas, fibrosarcomas and 9L gliomas. It was shown that Cu-ATSM is a valid PET hypoxia marker in some tumour types, but not for all; this tumour type-dependent hypoxia selectivity of Cu-ATSM challenges the use of Cu-ATSM as a universal PET hypoxia marker [131]. Cu-ATSM has a higher uptake in hypoxic tissues than the nitroimidazoles, allowing for high-quality images as soon as 20 min after injection [130, 132, 133]. ATSM is also flexible in that it can be labelled with any of several positron-emitting copper radioisotopes. Cu-ATSM has been used in a small number of human clinical trials, but no applications in human gliomas have yet been reported [134–136].

Other radionuclide agents

Recently, several other PET agents have been assessed for tumour hypoxia imaging: ^{99m}Tc- and ^{68}Ga-labelled metronidazole (MN), ^{99m}Tc-labelled iminodiacetic acid (IDA) derivative of 2-methyl-5-nitroimidazole and 1-(2-[^{18}F] fluoro-1-[hydroxymethyl]ethoxy)methyl-2-nitroimidazole, a ^{18}F-labelled 2-nitroimidazole analogue [137–139]. The last of these agents, 1-(2-[^{18}F]fluoro-1-[hydroxymethyl]ethoxy)methyl-2-nitroimidazole (FRP-170), was used to visualise hypoxic tissues in eight patients with glioma (three GBM, two oligodendroglioma and one each with diffuse astrocytoma, anaplastic ganglioglioma, and recurrent anaplastic astrocytoma). The FRP-170 PET images showed marked uptake with upregulation of HIF-1α in the three GBM, and moderate uptake in the recurrent anaplastic astrocytoma and one oligodendroglioma, but no uptake in the other tumours. The FRP-170 PET images showed positive correlation with HIF-1α immunoreactivity and some correlation with FDG PET and MRI enhancement (Figure 3), but no correlation with [^{11}C]-methionine PET. Imaging with FRP-170 PET also seemed

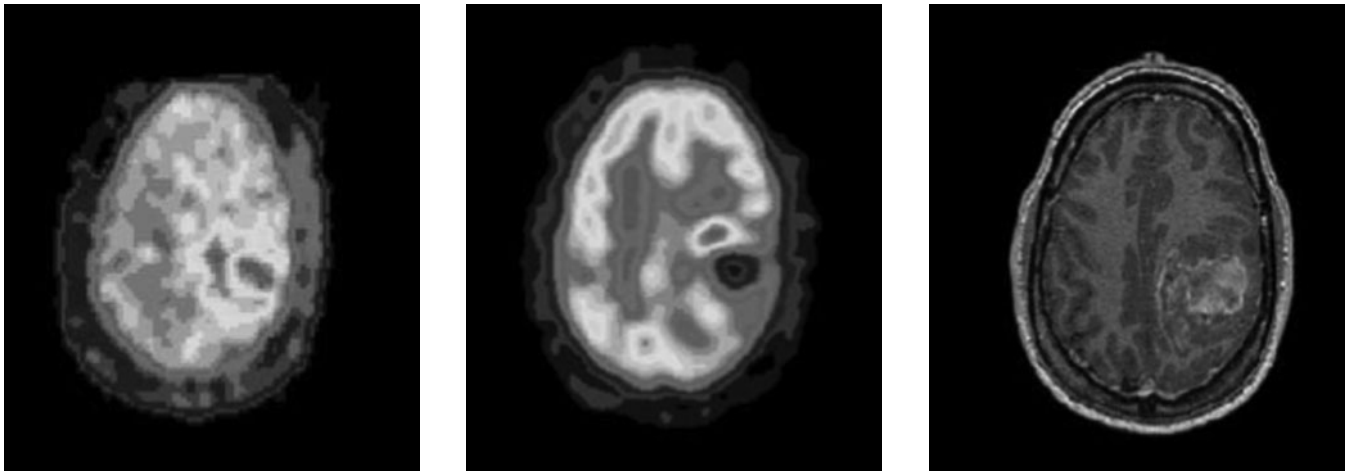

(a) (b) (c)

Figure 2. High-grade glioma (grade IV). (a) ^{18}F-labelled fluoro-misonidazole (^{18}F-MISO) positron emission tomography (PET). (b) ^{18}F-fluorodeoxyglucose (FDG) PET. (c) MRI. ^{18}F-FDG and ^{18}F-MISO uptake is evident in the left posterior parietal glioma, with uptake absent in the central necrotic area, although different patterns of maximal glucose metabolic rate and hypoxia are evident. Reproduced with permission from [128].

to be more sensitive for detecting hypoxia than identifying the lactate peak on proton MR spectroscopy [139].

All these agents are in their initial phases for research applications and none of them have been used in routine clinical imaging.

Magnetic resonance imaging

Advanced MRI techniques can be used to measure tumour perfusion and indirectly provide insights into hypoxia and angiogenesis in malignant tissues [37, 140–147]. Several MRI techniques are available, including DCE-MRI, which allows measurements of microvascular properties, magnetic resonance spectroscopy (MRS), which measures metabolite ratios, MR diffusion imaging and blood oxygen level-dependent MRI [148]. DCE-MRI uses paramagnetic contrast agents injected into the bloodstream and pharmacokinetic models of tumour contrast uptake over time to measure tumour perfusion and vascularity [149–155]. Several studies have shown DCE-MRI can be used to determine intratumoural blood flow and predict vascular permeability [143, 147, 149, 153]. Recently, advances in MR technology have enabled complex acquisitions of multiparametric data in gliomas, allowing complementary information to be obtained from the above-mentioned MRI techniques [148].

Blood oxygenation level dependent MRI

BOLD-MRI, also known as intrinsic susceptibility-weighted MRI, is a non-invasive MRI technique to indirectly measure oxygenation changes in tissues. In BOLD-MRI tissue contrast is affected by the intrinsic tissue properties (spin–lattice and spin–spin relaxations) and also by blood flow and paramagnetic deoxyhaemoglobin within red blood cells (in contrast to oxyhaemoglobin, which is not paramagnetic).

Deoxyhaemoglobin increases the MR transverse relaxation rate (R_2*), the inverse of the transverse relaxation time (T_2*), of water in blood and surrounding tissues. Thus, BOLD-MRI is sensitive to changes in pO_2 within vessels and in tissues adjacent to perfused vessels [156]. Susceptibility weighted images are also affected by iron content (*e.g.* myoglobin found in muscle), blood flow, carbon dioxide tension, haematocrit, pH and the presence of fibrosis or ligamentous structures (*e.g.* in benign prostatic hyperplasia and the suspensory ligaments of the breasts). To distinguish between the effects of flow from deoxyhaemoglobin and static tissue components, the T_2* relaxation rate (R_2*=1/T_2*) has to be measured. This can be done by using a multi-echo GRE sequence, sensitive to variations in the properties of the local magnetic field. Decoupling of flow from static effects on R_2* images occurs because the flow component can be thought of as affecting individual T_2* images of a multigradient echo sequence. Although synthetic R_2* images are free of blood flow contribution, reflecting mainly deoxyhaemoglobin content and static tissue components, improved blood flow and vascular function will also increase tissue oxygenation, which can be seen by changes in R_2* images.

BOLD-MRI images are more likely to reflect acute (perfusion-related) tissue hypoxia, due to transient occlusions of small blood vessels, while chronic hypoxia is less likely to be reflected by BOLD-MRI because of a greater distance between the red blood cells in the vessels and the area of hypoxic tissue. BOLD-MRI can only provide accurate information on tissue oxygenation if red blood cells are delivered to the tissue of interest. Human and xenograft studies have shown tumour perfusion varies widely and capillary blood delivery is not simply related to the absence/presence of vessels [157]. This observation could explain, in part, why no direct correlations between baseline R_2* and tissue pO_2 have been observed. Tissue oxygenation status can be accurately interpreted from R_2* images only if the distribution of blood volume in the tissue is known or experimentally determined. Thus, if a tissue is perfused and has a homogeneous blood volume fraction but has a high baseline R_2* in one area compared with another

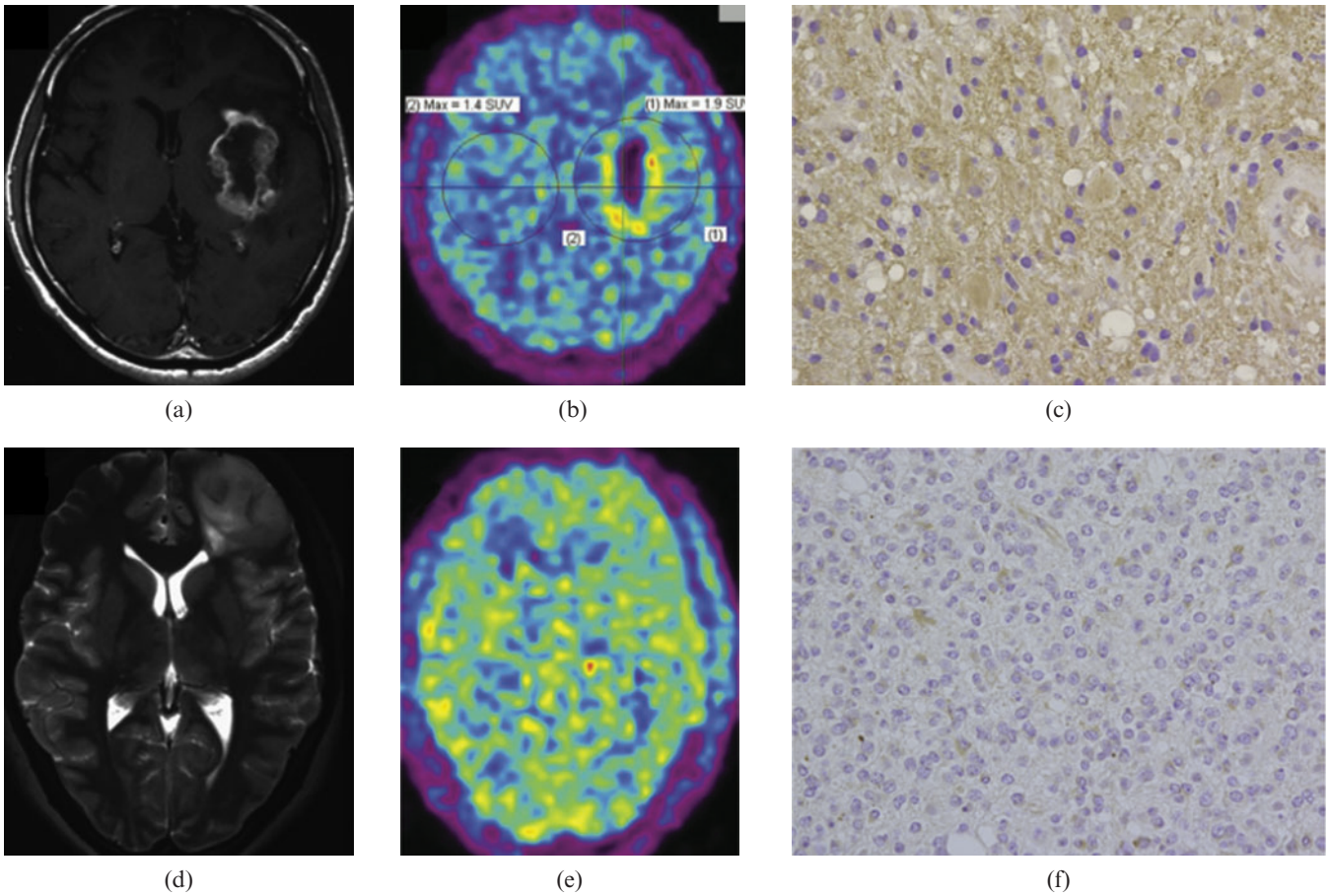

Figure 3. (a–c) A 68-year-old man with a glioblastoma multiforme (GBM). Axial T_1 weighted gadolinium-enhanced MR image (a) showing ring enhancement in the left insula, FRP-170 positron emission tomography (PET) image (b) showing marked uptake, and photomicrograph with hypoxia inducible factor-1α (HIF-1α) antibody (c) indicating strong immunoreactivity. Axial T_2 weighted MR image (d) showing a diffuse infiltrative lesion in the left frontal lobe, FRP-170 PET image (e) showing moderate uptake within the lesion, and photomicrograph with HIF-1α antibody (f) showing moderate immunoreactivity. Reproduced with permission from [139].

area in the same tissue, it can be inferred the high R_2* region is relatively more hypoxic; this hypothesis is supported by recent pre-clinical and clinical data [158].

The use of BOLD-MRI to evaluate tissue hypoxia is based on the assumption that haemoglobin oxygenation is proportional to blood arterial pO_2 which, in turn, is in equilibrium with the tissue oxygenation. Although changes in R_2* in response to vasomodulation with carbogen (95% CO_2:5% O_2) inhalation are temporally correlated with changes in tissue pO_2, only 50–60% of human tumours show changes in R_2* after carbogen inhalation [159, 160]. These limited and heterogeneous responses can partially be attributed to different perfusion patterns within tumours and even when vessels are present, red blood cell transport along intratumoural vessels may not be effective [157]. Hypoxic tumours with high blood volume (due to high microvessel density coupled with large vessels) will not only have raised baseline R_2* values but are more likely to respond to carbogen, with subsequent large changes in R_2* and positive radiosensitisation. Hypoxic tumours with low blood volume (due to lower microvessel density or small vessels) will have lower baseline R_2* values and are less likely to respond to carbogen, with negligible changes in R_2* and radiosensitisation with carbogen [161]. In these cases, BOLD response to carbogen is also dependent on the maturity of the underlying vasculature, with mature blood vessels being able to respond more actively to vasoconstrictory and vasodilatory stimuli [162].

The advantages of the BOLD-MRI technique are no need for externally administered contrast media or radioactive isotopes, easily repeatable and near real-time visualisation of time-dependent changes. BOLD-MRI is sensitive to the presence of changing vascular oxygen tension in the tissue and flow dependence of the MRI signal can also be decoupled. Major limitations of BOLD-MRI include the technique doesn't measure tissue pO_2 directly (either in blood or tissues because of a non-linear relationship of R_2* and tissue pO_2), the images obtained have low SNR and clinical studies with carbogen vasomodulation are technically challenging (approximately 25–35% of patient examinations fail due to respiratory distress caused by an increased respiratory drive induced by carbogen) [159, 160]. BOLD-MRI appears most sensitive to oxygen levels adjacent to perfused vessels (perfusion related or acute hypoxia) and BOLD-MRI sensitivity to more distant diffusion related (chronic hypoxia) is unknown.

Several studies explored the relationship between the BOLD-MRI signal and tumour oxygenation status in animal models and patients with gliomas. A recent study

in 9L and CNS-1 intracranial rat tumour models, before and during carbogen breathing, indicated glial sarcomas may be radiobiologically hypoxic, as evaluated by concurrent EPR oxymetry and BOLD-MRI measurements, and both techniques could reliably detect increases in brain tumour oxygenation after carbogen inhalation [163]. Hypoxic behaviour of cerebral gliomas has also been identified using BOLD-MRI in a small number of patients (six low grade, one high grade) during breath-holding [164]. The authors noted an absence of significant increase in the BOLD signal in both low-grade and high-grade gliomas, explained by either overwhelming hypoxia within the tumour, inadequacy or absence of hypercapnia-induced vasodilatation of tumour vessels, or both. Breath-hold regulated decreases in BOLD signals occurred only in the high-grade glioma, which is most likely due to the hypercapnia-induced steal effect that redistributes blood flow from tumour regions with unresponsive neovasculature to surrounding normal tissue. Another study looked at tumour heterogeneity and carbogen response in four patients with GBM and one patient with grade II astrocytoma [165]. The glioblastomas showed strong but heterogeneous signal changes between carbogen and air breathing, especially in the peritumoural areas corresponding to high-signal regions on T_2 weighted images, while the astrocytoma displayed a signal decrease during carbogen breathing in the peritumoural regions. The authors concluded that BOLD-MRI provides high-resolution images of cerebral anatomy and venous vascularisation and the technique, combined with hypercapnia challenge, allows for regional assessment of brain tumours.

Other studies have shown malignancies in the brain (meningiomas, gliomas or metastasis) can be distinguished from normal brain tissues using BOLD-MRI and in older patients with grade IV gliomas, BOLD signal intensity is equivalent to that measured in younger patients with grade IV gliomas, whereas in patients with grade II and III gliomas, BOLD-MRI signal change correlated only with increasing age [166, 167].

Oxygen-enhanced MRI

Since molecular oxygen is paramagnetic, elevated concentrations of oxygen dissolved in blood, plasma and tissue fluid increase the longitudinal relaxation rate ($R1=1/T_1$) via dipolar interactions. This effect has been quantified on T_1 weighted imaging in studies of normal tissue [168–173], emphysema [174] and tumours [175]. In contrast, T_2* weighted sequences are sensitive to changes in oxygenation status by an entirely different mechanism. Here, paramagnetic deoxygenated haemoglobin, compartmentalised in red blood cells, creates local variation in magnetic susceptibility, increasing the effective transverse relaxation rate ($R_2^*=1/T_2^*$) of vascular and perivascular water. The effects of breathing carbogen (95% oxygen and 5% carbon dioxide) and other hyperoxic hypercarbic gases on R_2* have been evaluated in normal tissue [159, 171, 176] and tumours [159, 172].

An oxygen-induced change in R1 is thought to reflect chiefly the amount of supraphysiological levels of dissolved oxygen in plasma and tissue fluid. Changes in arterial blood volume may modulate this effect, especially when carbogen is inhaled [172, 177]. A marked reduction in R_2* has been reported in several studies of diseased vasculature on carbogen inhalation, which may be dependent on vessel calibre [157], blood flow and blood volume effects [156, 177]. In distinction, breathing 100% oxygen has been reported to have a negligible effect on R_2* in normal tissues outside the brain [171]. In normal tissue, significant reductions in R1 were demonstrated following both oxygen and carbogen inhalation in the spleen, liver, skeletal muscle and renal cortex. No significant changes in R_2* occur with oxygen alone. In patients with advanced cancer in the abdomen and pelvis an oxygen inspiration challenge showed significant increases in R1 in the majority of cases [178]. Comparison with regional perfusion data showed congruence in most areas of the tumour, but some areas of mismatch with high levels of perfusion were not associated with significant changes in oxygen concentration. These observations support the use of oxygen-enhanced imaging as a biomarker for tumour oxygenation, although the relationship between the signal changes resulting from variations in dissolved oxygen pressure and true tumour hypoxaemia remain to be elucidated. Oxygen-enhanced imaging studies have not been applied in human brain tumours to date; however, studies in orthotopic tumours in the mouse brain showed close agreement between R_2* and R1 changes in response to oxygen inhalation [179].

Diffusion-weighted MRI

A study using diffusion MRI, an MRI technique that measures the mobility of water within tissues at a cellular level, in patients with high-grade gliomas, concluded that functional diffusion map analysis can provide a meaningful early assessment of treatment response in patients with high-grade gliomas [180]. Recently, bevacizumab-induced diffusion-restricted lesions have been reported in 18 patients with recurrent malignant gliomas before and after exposure to this drug [181]. These lesions were detectable as early as 4 weeks after initiation of therapy and were maintained for up to 80 weeks. Within the tumour bed, bevacizumab-induced diffusion-restricted lesions in the presence of reduced rCBF and rCBV. Although the cause of these alterations is unclear, it may involve atypical necrosis and chronic hypoxia. However, the relationship between hypoxia in gliomas and diffusion-weighted imaging measurements has not been explored in detail.

Dynamic contrast-enhanced MRI

DCE-MRI, using contrast agents of low molecular weight, may be used to estimate tumour parameters such as local perfusion and extracellular–extravascular volume [182]. Contrast agents generally contain chelates of gadolinium (Gd), which is an effective inducer of magnetic T_1 relaxation and thus induces an increase in signal intensity under T_1 weighted conditions.

Tumour vessels are highly disorganised, tortuous and dilated, uneven diameters, with biochemical and empirical concordance between vessel permeability and hypoxia [183, 184]. Imbalances of angiogenic mediators

such as VEGF and angiopoietins may contribute to this extensive branching and shunting. The excessive leakiness or hyperpermeability of tumour vessels is in part attributed to cytokines and angiogenic factors, which dynamically alter the structure of the microvessel walls [185].

It has been suggested DCE-MRI may be used as a surrogate for invasive pO_2 measurements [186]. Functional parameters derived from DCE-MRI have been shown to be related to pO_2 levels in murine tumours and correlate with microvessel density and tumour oxygenation in human cervix carcinomas [187–190]. Also, quantities derived from DCE-MRI have displayed a predictive value when evaluating the treatment response following radiotherapy of cervix cancers [191–193]. Furthermore, functional DCE-MRI images have been integrated in radiotherapy treatment planning in combination with morphological CT images [194].

^{1}H-magnetic resonance spectroscopy

^{1}H-magnetic resonance spectroscopy can provide useful metabolic information for brain tumour diagnosis and glioma grading [195, 196]. Two metabolites, lipids and lactates, both of which are present on short- and long-echo time (TE) sequences, have been studied as hypoxia markers. Lipids, which are related to necrosis, also represent an early response to cellular hypoxic stress [197–199]. The relationship between lipids and glioma grade is well established [196, 200]. The significance of lactates, which are the end product of anaerobic metabolism, in grading is more controversial [195, 200–203]. Either lipid or lactate signals have been identified in hypoxic areas and have been correlated with the rCBV in malignant gliomas [204]. Interestingly, in short-TE acquisitions, which are more able to detect mobile lipid droplets, some LGGs demonstrated small lipid peaks [195, 200, 205, 206]. To date, the predictive value of such peaks in LGGs for early angiogenesis switching and poor clinical outcome remains to be established, mainly by multivoxel sequences that can demonstrate glioma spatial heterogeneity.

Conclusions

Hypoxia probably plays a role in the development, angiogenesis and growth of malignant brain tumours; its impact in benign tumours is less clear. More research, especially regarding methods of measuring tumour hypoxia directly or—even more attractively—indirectly through imaging modalities, is necessary. Hypoxia is a logical therapeutic target for selective GBM because there are several ingenious methods to exploit tumour hypoxia available, but much more work will be required. An understanding of the role of hypoxia in tumour development and growth is important for physicians involved in the care of patients with brain tumours.

References

1. Vaupel P. The role of hypoxia-induced factors in tumor progression. Oncologist 2004;9:10–17.
2. Brown JM. The hypoxic cell: a target for selective cancer therapy—eighteenth Bruce F Cain Memorial Award lecture. Cancer Res 1999;59:5863–70.
3. Vaupel P, Harrison L. Tumor hypoxia: causative factors, compensatory mechanisms, and cellular response. Oncologist 2004;9:4–9.
4. Sundfor K, Lyng H, Rofstad EK. Tumour hypoxia and vascular density as predictors of metastasis in squamous cell carcinoma of the uterine cervix. Br J Cancer 1998;78:822–7.
5. Hockel M, Schlenger K, Hockel S, et al. Tumor hypoxia in pelvic recurrences of cervical cancer. Int J Cancer 1998;79:365–9.
6. Sanna K, Rofstad EK. Hypoxia-induced resistance to doxorubicin and methotrexate in human melanoma cell lines *in vitro*. Int J Cancer 1994;58:258–62.
7. Gatenby RA, Kessler HB, Rosenblum JS, et al. Oxygen distribution in squamous cell carcinoma metastases and its relationship to outcome of radiation therapy. Int J Radiat Oncol Biol Phys 1988;14:831–8.
8. Rice GC, Hoy C, Schimke RT. Transient hypoxia enhances the frequency of dihydrofolate reductase gene amplification in Chinese hamster ovary cells. Proc Natl Acad Sci USA 1986;83:5978–82.
9. Wilson RE, Keng PC, Sutherland RM. Drug resistance in Chinese hamster ovary cells during recovery from severe hypoxia. J Natl Cancer Inst 1989;81:1235–40.
10. Cuvier C, Jang A, Hill RP. Exposure to hypoxia, glucose starvation and acidosis: effect on invasive capacity of murine tumor cells and correlation with cathepsin (L + B) secretion. Clin Exp Metastasis 1997;15:19–25.
11. Graham CH, Forsdike J, Fitzgerald CJ, et al. Hypoxia-mediated stimulation of carcinoma cell invasiveness via upregulation of urokinase receptor expression. Int J Cancer 1999;80:617–23.
12. Walenta S, Wetterling M, Lehrke M, et al. High lactate levels predict likelihood of metastases, tumor recurrence, and restricted patient survival in human cervical cancers. Cancer Res 2000;60:916–21.
13. Hockel M, Schlenger K, Aral B, et al. Association between tumor hypoxia and malignant progression in advanced cancer of the uterine cervix. Cancer Res 1996;56:4509–15.
14. Graeber TG, Osmanian C, Jacks T, et al. Hypoxia-mediated selection of cells with diminished apoptotic potential in solid tumours. Nature 1996;379:88–91.
15. Eckerich C, Zapf S, Fillbrandt R, et al. Hypoxia can induce c-Met expression in glioma cells and enhance SF/HGF-induced cell migration. Int J Cancer 2007;121:276–83.
16. Jogi A, Ora I, Nilsson H, et al. Hypoxia alters gene expression in human neuroblastoma cells toward an immature and neural crest-like phenotype. Proc Natl Acad Sci USA 2002;99:7021–6.
17. Raza SM, Lang FF, Aggarwal BB, et al. Necrosis and glioblastoma: a friend or a foe? A review and a hypothesis. Neurosurgery 2002;51:2–12; discussion 12–13.
18. Russo CA, Weber TK, Volpe CM, et al. An anoxia inducible endonuclease and enhanced DNA breakage as contributors to genomic instability in cancer. Cancer Res 1995;55:1122–8.
19. Stoler DL, Anderson GR, Russo CA, et al. Anoxia-inducible endonuclease activity as a potential basis of the genomic instability of cancer cells. Cancer Res 1992;52:4372–8.
20. Sutherland RM. Tumor hypoxia and gene expression—implications for malignant progression and therapy. Acta Oncol 1998;37:567–74.
21. Hockel M, Vaupel P. Tumor hypoxia: definitions and current clinical, biologic, and molecular aspects. J Natl Cancer Inst 2001;93:266–76.
22. Powis G, Kirkpatrick L. Hypoxia inducible factor-1alpha as a cancer drug target. Mol Cancer Ther 2004;3:647–54.

23. Zhong H, De Marzo AM, Laughner E, et al. Overexpression of hypoxia-inducible factor 1alpha in common human cancers and their metastases. Cancer Res 1999;59:5830–5.
24. Beasley NJ, Leek R, Alam M, et al. Hypoxia-inducible factors HIF-1alpha and HIF-2alpha in head and neck cancer: relationship to tumor biology and treatment outcome in surgically resected patients. Cancer Res 2002;62:2493–7.
25. Volm M, Koomagi R. Hypoxia-inducible factor (HIF-1) and its relationship to apoptosis and proliferation in lung cancer. Anticancer Res 2000;20:1527–33.
26. Bos R, Zhong H, Hanrahan CF, et al. Levels of hypoxia-inducible factor-1 alpha during breast carcinogenesis. J Natl Cancer Inst 2001;93:309–14.
27. Leek RD, Talks KL, Pezzella F, et al. Relation of hypoxia-inducible factor-2 alpha (HIF-2 alpha) expression in tumor-infiltrative macrophages to tumor angiogenesis and the oxidative thymidine phosphorylase pathway in Human breast cancer. Cancer Res 2002;62:1326–9.
28. Jones A, Fujiyama C, Blanche C, et al. Relation of vascular endothelial growth factor production to expression and regulation of hypoxia-inducible factor-1 alpha and hypoxia-inducible factor-2 alpha in human bladder tumors and cell lines. Clin Cancer Res 2001;7:1263–72.
29. Akakura N, Kobayashi M, Horiuchi I, et al. Constitutive expression of hypoxia-inducible factor-1alpha renders pancreatic cancer cells resistant to apoptosis induced by hypoxia and nutrient deprivation. Cancer Res 2001;61: 6548–54.
30. Pugh CW, Ratcliffe PJ. Regulation of angiogenesis by hypoxia: role of the HIF system. Nat Med 2003;9:677–84.
31. Aebersold DM, Burri P, Beer KT, et al. Expression of hypoxia-inducible factor-1alpha: a novel predictive and prognostic parameter in the radiotherapy of oropharyngeal cancer. Cancer Res 2001;61:2911–16.
32. Birner P, Schindl M, Obermair A, et al. Overexpression of hypoxia-inducible factor 1alpha is a marker for an unfavorable prognosis in early-stage invasive cervical cancer. Cancer Res 2000;60:4693–6.
33. Bos R, van der Groep P, Greijer AE, et al. Levels of hypoxia-inducible factor-1alpha independently predict prognosis in patients with lymph node negative breast carcinoma. Cancer 2003;97:1573–81.
34. Pennacchietti S, Michieli P, Galluzzo M, et al. Hypoxia promotes invasive growth by transcriptional activation of the met protooncogene. Cancer Cell 2003;3:347–61.
35. Ruan H, Su H, Hu L, et al. A hypoxia-regulated adeno-associated virus vector for cancer-specific gene therapy. Neoplasia 2001;3:255–63.
36. Staller P, Sulitkova J, Lisztwan J, et al. Chemokine receptor CXCR4 downregulated by von Hippel-Lindau tumour suppressor pVHL. Nature 2003;425:307–11.
37. Carmeliet P, Dor Y, Herbert JM, et al. Role of HIF-1α in hypoxia-mediated apoptosis, cell proliferation and tumour angiogenesis. Nature 1998;394:485–90.
38. Maxwell PH, Dachs GU, Gleadle JM, et al. Hypoxia-inducible factor-1 modulates gene expression in solid tumors and influences both angiogenesis and tumor growth. Proc Natl Acad Sci USA 1997;94:8104–9.
39. Ryan HE, Lo J, Johnson RS. HIF-1 alpha is required for solid tumor formation and embryonic vascularization. EMBO J 1998;17:3005–15.
40. Ryan HE, Poloni M, McNulty W, et al. Hypoxia-inducible factor-1alpha is a positive factor in solid tumor growth. Cancer Res 2000;60:4010–15.
41. Jensen RL. Hypoxia in the tumorigenesis of gliomas and as a potential target for therapeutic measures. Neurosurg Focus 2006;20:E24.
42. Lal A, Peters H, St Croix B, et al. Transcriptional response to hypoxia in human tumors. J Natl Cancer Inst 2001;93: 1337–43.
43. Zundel W, Schindler C, Haas-Kogan D, et al. Loss of PTEN facilitates HIF-1-mediated gene expression. Genes Dev 2000;14:391–6.
44. Gaddipati JP, Madhavan S, Sidhu GS, et al. Picroliv—a natural product protects cells and regulates the gene expression during hypoxia/reoxygenation. Mol Cell Biochem 1999;194: 271–81.
45. Kimura H, Weisz A, Kurashima Y, et al. Hypoxia response element of the human vascular endothelial growth factor gene mediates transcriptional regulation by nitric oxide: control of hypoxia-inducible factor-1 activity by nitric oxide. Blood 2000;95:189–97.
46. Cooper R, Sarioglu S, Sokmen S, et al. Glucose transporter-1 (GLUT-1): a potential marker of prognosis in rectal carcinoma? Br J Cancer 2003;89:870–6.
47. Potter CP, Harris AL. Diagnostic, prognostic and therapeutic implications of carbonic anhydrases in cancer. Br J Cancer 2003;89:2–7.
48. Span PN, Bussink J, Manders P, et al. Carbonic anhydrase-9 expression levels and prognosis in human breast cancer: association with treatment outcome. Br J Cancer 2003;89: 271–6.
49. Flynn JR, Wang L, Gillespie DL, et al. Hypoxia-regulated protein expression, patient characteristics, and preoperative imaging as predictors of survival in adults with glioblastoma multiforme. Cancer 2008;113:1032–42.
50. Ihnatko R, Kubes M, Takacova M, et al. Extracellular acidosis elevates carbonic anhydrase IX in human glioblastoma cells via transcriptional modulation that does not depend on hypoxia. Int J Oncol 2006;29:1025–33.
51. Lund EL, Hog A, Olsen MW, et al. Differential regulation of VEGF, HIF1alpha and angiopoietin-1, -2 and -4 by hypoxia and ionizing radiation in human glioblastoma. Int J Cancer 2004;108:833–8.
52. Sondergaard KL, Hilton DA, Penney M, et al. Expression of hypoxia-inducible factor 1alpha in tumours of patients with glioblastoma. Neuropathol Appl Neurobiol 2002;28:210–17.
53. Vidal S, Horvath E, Kovacs K, et al. Expression of hypoxia-inducible factor-1alpha (HIF-1α) in pituitary tumours. Histol Histopathol 2003;18:679–86.
54. Zagzag D, Zhong H, Scalzitti JM, et al. Expression of hypoxia-inducible factor 1alpha in brain tumors: association with angiogenesis, invasion, and progression. Cancer 2000;88:2606–18.
55. Belkaid A, Fortier S, Cao J, et al. Necrosis induction in glioblastoma cells reveals a new ''bioswitch'' function for the M T_1-MMP/G6PT signaling axis in proMMP-2 activation versus cell death decision. Neoplasia 2007;9:332–40.
56. Said HM, Polat B, Staab A, et al. Rapid detection of the hypoxia-regulated CA-IX and NDRG1 gene expression in different glioblastoma cells *in vitro*. Oncol Rep 2008; 20:413–19.
57. Tsukamoto H, Boado RJ, Pardridge WM, Differential expression in glioblastoma multiforme and cerebral hemangioblastoma of cytoplasmic proteins that bind two different domains within the 3′-untranslated region of the human glucose transporter 1 (GLUT1) messenger RNA. J Clin Invest 1996;97:2823–32.
58. Said HM, Hagemann C, Staab A, et al. Expression patterns of the hypoxia-related genes osteopontin, CA9, erythropoietin, VEGF and HIF-1α in human glioma *in vitro* and *in vivo*. Radiother Oncol 2007;83:398–405.
59. Sathornsumetee S, Cao Y, Marcello JE, et al. Tumor angiogenic and hypoxic profiles predict radiographic response and survival in malignant astrocytoma patients treated with bevacizumab and irinotecan. J Clin Oncol 2008;26:271–8.
60. Gilhuis HJ, Bernse HJ, Jeuken JW, et al. The relationship between genetic aberrations as detected by comparative

genomic hybridization and vascularization in glioblastoma xenografts. J Neurooncol 2001;51:121–7.
61. Burton TR, Henson ES, Baijal P, et al. The pro-cell death Bcl-2 family member, BNIP3, is localized to the nucleus of human glial cells: Implications for glioblastoma multiforme tumor cell survival under hypoxia. Int J Cancer 2006;118: 1660–9.
62. Fischer U, Radermacher J, Mayer J, et al. Tumor hypoxia: Impact on gene amplification in glioblastoma. Int J Oncol 2008;33:509–15.
63. Rak J, Filmus J, Finkenzeller G, et al. Oncogenes as inducers of tumor angiogenesis. Cancer Metastasis Rev 1995;14: 263–77.
64. Giaccia AJ. Hypoxic stress proteins: survival of the fittest. Semin Radiat Oncol 1996;6:46–58.
65. Hanahan D, Folkman J. Patterns and emerging mechanisms of the angiogenic switch during tumorigenesis. Cell 1996;86:353–64.
66. Kerbel RS, Viloria-Petit A, Okada F, et al. Establishing a link between oncogenes and tumor angiogenesis. Mol Med 1998;4:286–95.
67. Louis DN, Gusella JF. A tiger behind many doors: multiple genetic pathways to malignant glioma. Trends Genet 1995;11:412–15.
68. Li JL, Sainson RC, Shi W, et al. Delta-like 4 Notch ligand regulates tumor angiogenesis, improves tumor vascular function, and promotes tumor growth *in vivo*. Cancer Res 2007;67:11244–53.
69. Blasberg RG, Kobayashi T, Horowitz M, et al. Regional blood flow in ethylnitrosourea-induced brain tumors. Ann Neurol 1983;14:189–201.
70. Groothuis DR, Pasternak JF, Fischer JM, et al. Regional measurements of blood flow in experimental RG-2 rat gliomas. Cancer Res 1983;43:3362–7.
71. Hossman KA, Bloink M. Blood flow and regulation of blood flow in experimental peritumoral edema. Stroke 1981;12: 211–17.
72. Jain RK. Determinants of tumor blood flow: a review. Cancer Res 1988;48:2641–58.
73. Vajkoczy P, Menger MD. Vascular microenvironment in gliomas. Cancer Treat Res 2004;117:249–62.
74. Groshar D, McEwan AJ, Parliament MB, et al. Imaging tumor hypoxia and tumor perfusion. J Nucl Med 1993; 34:885–8.
75. Parliament MB, Franko AJ, Allalunis-Turner MJ, et al. Anomalous patterns of nitroimidazole binding adjacent to necrosis in human glioma xenografts: possible role of decreased oxygen consumption. Br J Cancer 1997;75:311–18.
76. Rampling R, Cruickshank G, Lewis AD, et al. Direct measurement of pO2 distribution and bioreductive enzymes in human malignant brain tumors. Int J Radiat Oncol Biol Phys 1994;29:427–31.
77. Valk PE, Mathis CA, Prados MD, et al. Hypoxia in human gliomas: demonstration by PET with fluorine-18-fluoromisonidazole. J Nucl Med 1992;33:2133–7.
78. Raza SM, Fuller GN, Rhee CH, et al. Identification of necrosis-associated genes in glioblastoma by cDNA microarray analysis. Clin Cancer Res 2004;10:212–21.
79. Rong Y, Durden DL, Van Meir EG, et al. 'Pseudopalisading' necrosis in glioblastoma: a familiar morphologic feature that links vascular pathology, hypoxia, and angiogenesis. J Neuropathol Exp Neurol 2006;65:529–39.
80. Brat DJ, Castellano-Sanchez AA, Hunter SB, et al. Pseudopalisades in glioblastoma are hypoxic, express extracellular matrix proteases, and are formed by an actively migrating cell population. Cancer Res 2004;64:920–7.
81. Zagzag D, Esencay M, Mendez O, et al. Hypoxia- and vascular endothelial growth factor-induced stromal cell-derived factor-1alpha/CXCR4 expression in glioblastomas: one plausible explanation of Scherer's structures. Am J Pathol 2008;173:545–60.
82. Zagzag D, Lukyanov Y, Lan L, et al. Hypoxia-inducible factor 1 and VEGF upregulate CXCR4 in glioblastoma: implications for angiogenesis and glioma cell invasion. Lab Invest 2006;86:1221–32.
83. Elstner A, Holtkamp N, von Deimling A. Involvement of Hif-1 in desferrioxamine-induced invasion of glioblastoma cells. Clin Exp Metastasis 2007;24:57–66.
84. Mirimanoff RO. The evolution of chemoradiation for glioblastoma: a modern success story. Curr Oncol Rep 2006;8:50–3.
85. Stupp R, Weber DC. The role of radio- and chemotherapy in glioblastoma. Onkologie 2005;28:315–17.
86. Chen Z, Htay A, Dos Santos W, et al. In vitro, angiogenesis by human umbilical vein endothelial cells (HUVEC) induced by three-dimensional co-culture with glioblastoma cells. J Neurooncol 2009;92:121–8.
87. Merighi S, Benini A, Mirandola P, et al. Hypoxia inhibits paclitaxel-induced apoptosis through adenosine-mediated phosphorylation of bad in glioblastoma cells. Mol Pharmacol 2007;72:162–72.
88. Ezhilarasan R, Mohanam I, Govindarajan K, et al. Glioma cells suppress hypoxia-induced endothelial cell apoptosis and promote the angiogenic process. Int J Oncol 2007;30: 701–7.
89. Leibel SA, Scott CB, Loeffler JS. Contemporary approaches to the treatment of malignant gliomas with radiation therapy. Semin Oncol 1994;21:198–219.
90. Stieber VW, Mehta MP. Advances in radiation therapy for brain tumors. Neurol Clin 2007;25:1005–33, ix.
91. Padhani AR, Krohn KA, Lewis JS, et al. Imaging oxygenation of human tumours. Eur Radiol 2007;17:861–72.
92. Bloom HJ. Intracranial tumors: response and resistance to therapeutic endeavors, 1970–1980. Int J Radiat Oncol Biol Phys 1982;8:1083–113.
93. Eyler CE, Rich JN. Survival of the fittest: cancer stem cells in therapeutic resistance and angiogenesis. J Clin Oncol 2008;26: 2839–45.
94. Spence AM, Muzi M, Swanson KR, et al. Regional hypoxia in glioblastoma multiforme quantified with [18F] fluoromisonidazole positron emission tomography before radiotherapy: correlation with time to progression and survival. Clin Cancer Res 2008;14:2623–30.
95. Bussink J, Kaanders JH, van der Kogel AJ. Tumor hypoxia at the micro-regional level: clinical relevance and predictive value of exogenous and endogenous hypoxic cell markers. Radiother Oncol 2003;67:3–15.
96. Williams KJ, Parker CA, Stratford IJ. Exogenous and endogenous markers of tumour oxygenation status: definitive markers of tumour hypoxia? Adv Exp Med Biol 2005;566:285–94.
97. Kaynar MY, Sanus GZ, Hnimoglu H, et al. Expression of hypoxia inducible factor-1alpha in tumors of patients with glioblastoma multiforme and transitional meningioma. J Clin Neurosci 2008;15:1036–42.
98. Lord EM, Harwell L, Koch CJ. Detection of hypoxic cells by monoclonal antibody recognizing 2-nitroimidazole adducts. Cancer Res 1993;53:5721–6.
99. Arteel GE, Thurman RG, Raleigh JA. Reductive metabolism of the hypoxia marker pimonidazole is regulated by oxygen tension independent of the pyridine nucleotide redox state. Eur J Biochem 1998;253:743–50.
100. Rijken PF, Bernsen HJ, Peters JP, et al. Spatial relationship between hypoxia and the (perfused) vascular network in a human glioma xenograft: a quantitative multi-parameter analysis. Int J Radiat Oncol Biol Phys 2000;48:571–82.
101. Raleigh JA, Chou SC, Arteel GE, et al. Comparisons among pimonidazole binding, oxygen electrode measurements,

and radiation response in C3H mouse tumors. Radiat Res 1999;151:580–9.
102. Wijffels KI, Kaanders JH, Rijken PF, et al. Vascular architecture and hypoxic profiles in human head and neck squamous cell carcinomas. Br J Cancer 2000;83: 674–83.
103. Raleigh JA, Chou SC, Calkins-Adams DP, et al. A clinical study of hypoxia and metallothionein protein expression in squamous cell carcinomas. Clin Cancer Res 2000;6: 855–62.
104. Vukovic V, Haugland HK, Nicklee T, et al. Hypoxia-inducible factor-1alpha is an intrinsic marker for hypoxia in cervical cancer xenografts. Cancer Res 2001;61:7394–8.
105. Tatum JL, Kelloff GJ, Gillies RJ, et al. Hypoxia: importance in tumor biology, noninvasive measurement by imaging, and value of its measurement in the management of cancer therapy. Int J Radiat Biol 2006;82:699–757.
106. Bentzen L, Keiding S, Nordsmark M, et al. Tumour oxygenation assessed by 18F-fluoromisonidazole PET and polarographic needle electrodes in human soft tissue tumours. Radiother Oncol 2003;67:339–44.
107. Collingridge DR, Piepmeier JM, Rockwell S, et al. Polarographic measurements of oxygen tension in human glioma and surrounding peritumoural brain tissue. Radiother Oncol 1999;53:127–31.
108. Helmlinger G, Yuan F, Dellian M, et al. Interstitial pH and pO2 gradients in solid tumors *in vivo*: high-resolution measurements reveal a lack of correlation. Nat Med 1997;3:177–82.
109. Kallinowski F, Zander R, Hoeckel M, et al. Tumor tissue oxygenation as evaluated by computerized-pO2-histography. Int J Radiat Oncol Biol Phys 1990;19:953–61.
110. Kayama T, Yoshimoto T, Fujimoto S, et al. Intratumoral oxygen pressure in malignant brain tumor. J Neurosurg 1991;74:55–9.
111. Doll CM, Milosevic M, Pintilie M, et al. Estimating hypoxic status in human tumors: a simulation using Eppendorf oxygen probe data in cervical cancer patients. Int J Radiat Oncol Biol Phys 2003;55:1239–46.
112. Riesterer O, Milas L, Ang KK. Use of molecular biomarkers for predicting the response to radiotherapy with or without chemotherapy. J Clin Oncol 2007;25:4075–83.
113. Vordermark D, Brown JM. Evaluation of hypoxia-inducible factor-1alpha (HIF-1α) as an intrinsic marker of tumor hypoxia in U87 MG human glioblastoma: *in vitro* and xenograft studies. Int J Radiat Oncol Biol Phys 2003; 56:1184–93.
114. Airley RE, Loncaster J, Raleigh JA, et al. GLUT-1 and CAIX as intrinsic markers of hypoxia in carcinoma of the cervix: relationship to pimonidazole binding. Int J Cancer 2003;104:85–91.
115. Loncaster JA, Harris AL, Davidson SE, et al. Carbonic anhydrase (CA IX) expression, a potential new intrinsic marker of hypoxia: correlations with tumor oxygen measurements and prognosis in locally advanced carcinoma of the cervix. Cancer Res 2001;61:6394–9.
116. Wykoff CC, Beasley NJ, Watson PH, et al. Hypoxia-inducible expression of tumor-associated carbonic anhydrases. Cancer Res 2000;60:7075–83.
117. Olive PL, Aquino-Parsons C, MacPhail SH, et al. Carbonic anhydrase 9 as an endogenous marker for hypoxic cells in cervical cancer. Cancer Res 2001;61:8924–9.
118. Brown JM, Le QT. Tumor hypoxia is important in radiotherapy, but how should we measure it? Int J Radiat Oncol Biol Phys 2002;54:1299–301.
119. Bruehlmeier M, Roelcke U, Schubiger PA, et al. Assessment of hypoxia and perfusion in human brain tumors using PET with 18F-fluoromisonidazole and 15O-H2O. J Nucl Med 2004;45:1851–9.
120. Rischin D, Peters L, Hicks R, et al. Phase I trial of concurrent tirapazamine, cisplatin, and radiotherapy in patients with advanced head and neck cancer. J Clin Oncol 2001;19:535–42.
121. Tochon-Danguy HJ, Sachinidis JI, Chan F, et al. Imaging and quantitation of the hypoxic cell fraction of viable tumor in an animal model of intracerebral high grade glioma using [18F]fluoromisonidazole (FMISO). Nucl Med Biol 2002;29:191–7.
122. Rasey JS, Casciari JJ, Hofstrand PD, et al. Determining hypoxic fraction in a rat glioma by uptake of radiolabeled fluoromisonidazole. Radiat Res 2000;153:84–92.
123. Rasey JS, Hofstrand PD, Chin LK, et al. Characterization of [18F]fluoroetanidazole, a new radiopharmaceutical for detecting tumor hypoxia. J Nucl Med 1999;40:1072–9.
124. Rasey JS, Koh WJ, Evans ML, et al. Quantifying regional hypoxia in human tumors with positron emission tomography of [18F]fluoromisonidazole: a pretherapy study of 37 patients. Int J Radiat Oncol Biol Phys 1996;36:417–28.
125. Martin GV, Caldwell JH, Rasey JS, et al. Enhanced binding of the hypoxic cell marker [3H]fluoromisonidazole in ischemic myocardium. J Nucl Med 1989;30:194–201.
126. Szeto MD, Chakraborty G, Hadley J, et al. Quantitative metrics of net proliferation and invasion link biological aggressiveness assessed by MRI with hypoxia assessed by FMISO-PET in newly diagnosed glioblastomas. Cancer Res 2009;69:4502–9.
127. Hicks RJ, Rischin D, Fisher R, et al. Utility of FMISO PET in advanced head and neck cancer treated with chemoradiation incorporating a hypoxia-targeting chemotherapy agent. Eur J Nucl Med Mol Imaging 2005;32:1384–91.
128. Cher LM, Murone C, Lawrentschuk N, et al. Correlation of hypoxic cell fraction and angiogenesis with glucose metabolic rate in gliomas using 18F-fluoromisonidazole, 18F-FDG PET, and immunohistochemical studies. J Nucl Med 2006;47:410–18.
129. Troost EG, Laverman P, Kaanders JH, et al. Imaging hypoxia after oxygenation-modification: comparing [18F] FMISO autoradiography with pimonidazole immunohistochemistry in human xenograft tumors. Radiother Oncol 2006;80:157–64.
130. Lewis JS, McCarthy DW, McCarthy TJ, et al. Evaluation of 64Cu-ATSM *in vitro* and *in vivo* in a hypoxic tumor model. J Nucl Med 1999;40:177–83.
131. Yuan H, Schroeder T, Bowsher JE, et al. Intertumoral differences in hypoxia selectivity of the PET imaging agent 64Cu(II)-diacetyl-bis(N4-methylthiosemicarbazone). J Nucl Med 2006;47:989–98.
132. Lewis JS, Sharp TL, Laforest R, et al. Tumor uptake of copper-diacetyl-bis(N(4)-methylthiosemicarbazone): effect of changes in tissue oxygenation. J Nucl Med 2001;42:655–61.
133. Obata A, Yoshimi E, Waki A, et al. Retention mechanism of hypoxia selective nuclear imaging/radiotherapeutic agent cu-diacetyl-bis(N4-methylthiosemicarbazone) (Cu-ATSM) in tumor cells. Ann Nucl Med 2001;15:499–504.
134. Blankenberg FG, Eckelman WC, Strauss HW, et al. Role of radionuclide imaging in trials of antiangiogenic therapy. Acad Radiol 2000;7:851–67.
135. Dehdashti F, Grigsby PW, Mintun MA, et al. Assessing tumor hypoxia in cervical cancer by positron emission tomography with 60Cu-ATSM: relationship to therapeutic response-a preliminary report. Int J Radiat Oncol Biol Phys 2003;55:1233–8.
136. Fujibayashi Y, Taniuchi H, Yonekura Y, et al. Copper-62-ATSM: a new hypoxia imaging agent with high membrane permeability and low redox potential. J Nucl Med 1997;38:1155–60.
137. Ito M, Yang DJ, Mawlawi O, et al. PET and planar imaging of tumor hypoxia with labeled metronidazole. Acad Radiol 2006;13:598–609.

138. Mallia MB, Subramanian S, Banerjee S, et al. Evaluation of 99mTc(CO)3 complex of 2-methyl-5-nitroimidazole as an agent for targeting tumor hypoxia. Bioorg Med Chem 2006;14:7666–70.
139. Shibahara I, Kumabe T, Kanamori M, et al. Imaging of hypoxic lesions in patients with gliomas by using positron emission tomography with 1-(2-[(18)F] fluoro-1-[hydroxymethyl]ethoxy)methyl-2-nitroimidazole, a new (18)F-labeled 2-nitroimidazole analog. J Neurosurg 2010;113:358–68.
140. Abramovitch R, Dafni H, Smouha E, et al. *In vivo* prediction of vascular susceptibility to vascular susceptibility endothelial growth factor withdrawal: magnetic resonance imaging of C6 rat glioma in nude mice. Cancer Res 1999;59:5012–16.
141. Abramovitch R, Marikovsky M, Meir G, et al. Stimulation of tumour angiogenesis by proximal wounds: spatial and temporal analysis by MRI. Br J Cancer 1998;77:440–7.
142. Brasch R, Pham C, Shames D, et al. Assessing tumor angiogenesis using macromolecular MR imaging contrast media. J Magn Reson Imaging 1997;7:68–74.
143. Daldrup H, Shames DM, Wendland M, et al. Correlation of dynamic contrast-enhanced MR imaging with histologic tumor grade: comparison of macromolecular and small-molecular contrast media. AJR Am J Roentgenol 1998; 171:941–9.
144. Gossmann A, Okuhata Y, Shames DM, et al. Prostate cancer tumor grade differentiation with dynamic contrast-enhanced MR imaging in the rat: comparison of macromolecular and small-molecular contrast media—preliminary experience. Radiology 1999;213:265–72.
145. Griffiths JR, Taylor NJ, Howe FA, et al. The response of human tumors to carbogen breathing, monitored by Gradient-Recalled Echo Magnetic Resonance Imaging. Int J Radiat Oncol Biol Phys 1997;39:697–701.
146. Knopp EA, Cha S, Johnson G, et al. Glial neoplasms: dynamic contrast-enhanced T_2*-weighted MR imaging. Radiology 1999;211:791–8.
147. Sugahara T, Korogi Y, Tomiguchi S, et al. Posttherapeutic intraaxial brain tumor: the value of perfusion-sensitive contrast-enhanced MR imaging for differentiating tumor recurrence from nonneoplastic contrast-enhancing tissue. AJNR Am J Neuroradiol 2000;21:901–9.
148. McMillan KM, Rogers BP, Field AS, et al. Physiologic characterisation of glioblastoma multiforme using MRI-based hypoxia mapping, chemical shift imaging, perfusion and diffusion maps. J Clin Neurosci 2006;13:811–17.
149. Bhujwalla ZM, Artemov D, Natarajan K, et al. Vascular differences detected by MRI for metastatic versus non-metastatic breast and prostate cancer xenografts. Neoplasia 2001;3:143–53.
150. Fisher MJ, Adamson PC. Anti-angiogenic agents for the treatment of brain tumors. Neuroimaging Clin N Am 2002;12:477–99.
151. McDonald DM, Choyke PL. Imaging of angiogenesis: from microscope to clinic. Nat Med 2003;9:713–25.
152. Pathak AP, Schmainda KM, Ward BD, et al. MR-derived cerebral blood volume maps: issues regarding histological validation and assessment of tumor angiogenesis. Magn Reson Med 2001;46:735–47.
153. Pham CD, Roberts TP, van Bruggen N, et al. Magnetic resonance imaging detects suppression of tumor vascular permeability after administration of antibody to vascular endothelial growth factor. Cancer Invest 1998;16:225–30.
154. Su MY, Najafi AA, Nalcioglu O. Regional comparison of tumor vascularity and permeability parameters measured by albumin-Gd-DTPA and Gd-DTPA. Magn Reson Med 1995;34:402–11.
155. Turetschek K, Roberts TP, Floyd E, et al. Tumor microvascular characterization using ultrasmall superparamagnetic iron oxide particles (USPIO) in an experimental breast cancer model. J Magn Reson Imaging 2001;13:882–8.
156. Howe FA, Robinson SP, McIntyre DJ, et al. Issues in flow and oxygenation dependent contrast (FLOOD) imaging of tumours. NMR Biomed 2001;14:497–506.
157. Robinson SP, Rijken PF, Howe FA, et al. Tumor vascular architecture and function evaluated by non-invasive susceptibility MRI methods and immunohistochemistry. J Magn Reson Imaging 2003;17:445–54.
158. Kostourou V, Robinson SP, Whitley GS, et al. Effects of overexpression of dimethylarginine dimethylaminohydrolase on tumor angiogenesis assessed by susceptibility magnetic resonance imaging. Cancer Res 2003;63:4960–6.
159. Taylor NJ, Baddeley H, Goodchild KA, et al. BOLD MRI of human tumor oxygenation during carbogen breathing. J Magn Reson Imaging 2001;14:156–63.
160. Rijpkema M, Kaanders JH, Joosten FB, et al. Effects of breathing a hyperoxic hypercapnic gas mixture on blood oxygenation and vascularity of head-and-neck tumors as measured by magnetic resonance imaging. Int J Radiat Oncol Biol Phys 2002;53:1185–91.
161. Rodrigues LM, Howe FA, Griffiths JR, et al. Tumor R_2* is a prognostic indicator of acute radiotherapeutic response in rodent tumors. J Magn Reson Imaging 2004;19:482–8.
162. Neeman M. Functional and molecular MR imaging of angiogenesis: seeing the target, seeing it work. J Cell Biochem Suppl 2002;39:11–17.
163. Dunn JF, O'Hara JA, Zaim-Wadghiri Y, et al. Changes in oxygenation of intracranial tumors with carbogen: a BOLD MRI and EPR oximetry study. J Magn Reson Imaging 2002;16:511–21.
164. Hsu YY, Chang CN, Jung SM, et al. Blood oxygenation level-dependent MRI of cerebral gliomas during breath holding. J Magn Reson Imaging 2004;19:160–7.
165. Rauscher A, Sedlacik J, Fitzek C, et al. High resolution susceptibility weighted MR-imaging of brain tumors during the application of a gaseous agent. Rofo 2005; 177:1065–9.
166. Chen CM, Hou BL, Holodny AI. Effect of age and tumor grade on BOLD functional MR imaging in preoperative assessment of patients with glioma. Radiology 2008;248:971–8.
167. Feldman SC, Chu D, Schulder M, et al. The blood oxygen level-dependent functional MR imaging signal can be used to identify brain tumors and distinguish them from normal tissue. AJNR Am J Neuroradiol 2009;30:389–95.
168. Gore JC. The meaning and significance of relaxation in NMR. Radiology 1982;142:243.
169. Edelman RR, Hatabu H, Tadamura E, et al. Noninvasive assessment of regional ventilation in the human lung using oxygen-enhanced magnetic resonance imaging. Nature Medicine 1996;2:1236–9.
170. Tadamura E, Hatabu H, Li W, et al. Effect of oxygen inhalation on relaxation times in various tissues. J Magn Reson Imaging 1997;7:220–5.
171. Jones RA, Ries M, Moonen CTW, et al. Imaging the changes in renal T-1 induced by the inhalation of pure oxygen: A feasibility study. Magn Reson Med 2002;47:728–35.
172. O'Connor JPB, Jackson A, Buonaccorsi GA, et al. Organ-specific effects of oxygen and carbogen gas inhalation on tissue longitudinal relaxation times. Magn Reson Med 2007;58:490–6.
173. McGrath DM, Naish JH, O'Connor JPB, et al. Oxygen-induced changes in longitudinal relaxation times in skeletal muscle. Magn Reson Imaging 2008;26:221–7.
174. Ohno Y, Hatabu H, Takenaka D, et al. Oxygen-enhanced MR ventilation imaging of the lung: Preliminary clinical experience in 25 subjects. AJR Am J Roentgenol 2001;177:185–94.
175. Arnold JFT, Kotas M, Fidler F, et al. Quantitative regional oxygen transfer Imaging of the human lung. J Magn Reson Imaging 2007;26:637–45.

176. Thulborn KR, Waterton JC, Matthews PM, et al. Oxygenation dependence of the transverse relaxation time of water protons in whole blood at high field. Biochim Biophys Acta 1982;714:265–70.
177. O'Connor JP, Naish JH, Jackson A, et al. Comparison of normal tissue R1 and R*2 modulation by oxygen and carbogen. Magn Reson Med 2009;61:75–83.
178. O'Connor JP, Naish JH, Parker GJ, et al. Preliminary study of oxygen-enhanced longitudinal relaxation in MRI: a potential novel biomarker of oxygenation changes in solid tumors. Int J Radiat Oncol Biol Phys 2009;75:1209–15.
179. Zhou HA, Mason RP, Zhao D. Integrated MRI Approaches to Interrogate Tumor Oxygenation and Vascular Perfusion of Orthotopic Brain Tumors in a Mouse Model. in ISMRM-ESMRMB Joint Annual Meeting. 2010. Stockholm, Sweden.
180. Compostella A, Tosoni A, Blatt V, et al. Prognostic factors for anaplastic astrocytomas. J Neurooncol 2007;81:295–303.
181. Rieger J, Bahr O, Muller K, et al. Bevacizumab-induced diffusion-restricted lesions in malignant glioma patients. J Neurooncol 2010;99:49–56.
182. Tofts PS, Brix G, Buckley DL, et al. Estimating kinetic parameters from dynamic contrast-enhanced T(1)-weighted MRI of a diffusable tracer: standardized quantities and symbols. J Magn Reson Imaging 1999;10:223–32.
183. Dewhirst MW, Tso CY, Oliver R, et al. Morphologic and hemodynamic comparison of tumor and healing normal tissue microvasculature. Int J Radiat Oncol Biol Phys 1989;17:91–9.
184. Dewhirst MW, Klitzman B, Braun RD, et al. Review of methods used to study oxygen transport at the microcirculatory level. Int J Cancer 2000;90:237–55.
185. Dvorak HF, Nagy JA, Feng D, et al. Vascular permeability factor/vascular endothelial growth factor and the significance of microvascular hyperpermeability in angiogenesis. Curr Top Microbiol Immunol 1999;237:97–132.
186. Foo SS, Abbott DF, Lawrentschuk N, et al. Functional imaging of intratumoral hypoxia. Mol Imaging Biol 2004;6:291–305.
187. Goda F, Bacic G, O'Hara JA, et al. The relationship between partial pressure of oxygen and perfusion in two murine tumors after X-ray irradiation: a combined gadopentetate dimeglumine dynamic magnetic resonance imaging and in vivo electron paramagnetic resonance oximetry study. Cancer Res 1996;56:3344–9.
188. Hawighorst H, Knapstein PG, Knopp MV, et al. Uterine cervical carcinoma: comparison of standard and pharmacokinetic analysis of time-intensity curves for assessment of tumor angiogenesis and patient survival. Cancer Res 1998;58:3598–602.
189. Cooper RA, Carrington BM, Loncaster JA, et al. Tumour oxygenation levels correlate with dynamic contrast-enhanced magnetic resonance imaging parameters in carcinoma of the cervix. Radiother Oncol 2000;57:53–9.
190. Lyng H, Vorren AO, Sundfor K, et al. Assessment of tumor oxygenation in human cervical carcinoma by use of dynamic Gd-DTPA-enhanced MR imaging. J Magn Reson Imaging 2001;14:750–6.
191. Mayr NA, Yuh WT, Arnholt JC, et al. Pixel analysis of MR perfusion imaging in predicting radiation therapy outcome in cervical cancer. J Magn Reson Imaging 2000; 12:1027–33.
192. Yamashita Y, Baba T, Baba Y, et al. Dynamic contrast-enhanced MR imaging of uterine cervical cancer: pharmacokinetic analysis with histopathologic correlation and its importance in predicting the outcome of radiation therapy. Radiology 2000;216:803–9.
193. Loncaster JA, Carrington BM, Sykes JR, et al. Prediction of radiotherapy outcome using dynamic contrast enhanced MRI of carcinoma of the cervix. Int J Radiat Oncol Biol Phys 2002;54:759–67.
194. Neff T, Kiessling F, Brix G, et al. An optimized workflow for the integration of biological information into radiotherapy planning: experiences with T_1w DCE-MRI. Phys Med Biol 2005;50:4209–23.
195. Kaminogo M, Ishimaru H, Morikawa M, et al. Diagnostic potential of short echo time MR spectroscopy of gliomas with single-voxel and point-resolved spatially localised proton spectroscopy of brain. Neuroradiology 2001;43: 353–63.
196. Poptani H, Gupta RK, Roy R, et al. Characterization of intracranial mass lesions with *in vivo* proton MR spectroscopy. AJNR Am J Neuroradiol 1995;16:1593–603.
197. Barba I, Cabanas ME, Arus C. The relationship between nuclear magnetic resonance-visible lipids, lipid droplets, and cell proliferation in cultured C6 cells. Cancer Res 1999;59:1861–8.
198. Lim M, Cheshier S, Steinberg GK. New vessel formation in the central nervous system during tumor growth, vascular malformations, and Moyamoya. Curr Neurovasc Res 2006;3:237–45.
199. Remy C, Fouilhe N, Barba I, et al. Evidence that mobile lipids detected in rat brain glioma by 1H nuclear magnetic resonance correspond to lipid droplets. Cancer Res 1997;57:407–14.
200. Fayed N, Morales H, Modrego PJ, et al. Contrast/Noise ratio on conventional MRI and choline/creatine ratio on proton MRI spectroscopy accurately discriminate low-grade from high-grade cerebral gliomas. Acad Radiol 2006;13:728–37.
201. Howe FA, Opstad KS. 1H MR spectroscopy of brain tumours and masses. NMR Biomed 2003;16:123–31.
202. Howe FA, Barton SJ, Cudlip SA, et al. Metabolic profiles of human brain tumors using quantitative *in vivo* 1H magnetic resonance spectroscopy. Magn Reson Med 2003;49:223–32.
203. Walecki J, Tarasow E, Kubas B, et al. Hydrogen-1 MR spectroscopy of the peritumoral zone in patients with cerebral glioma: assessment of the value of the method. Acad Radiol 2003;10:145–53.
204. Li X, Vigneron DB, Cha S, et al. Relationship of MR-derived lactate, mobile lipids, and relative blood volume for gliomas *in vivo*. AJNR Am J Neuroradiol 2005;26:760–9.
205. Jenkinson MD, Smith TS, Joyce K, et al. MRS of oligodendroglial tumors: correlation with histopathology and genetic subtypes. Neurology 2005;64:2085–9.
206. Rijpkema M, Schuuring J, van der Meulen Y, et al. Characterization of oligodendrogliomas using short echo time 1H MR spectroscopic imaging. NMR Biomed 2003; 16:12–18.